Hindawi
Shock and Vibration
Volume 2019, Article ID 8385310, 14 pages
https://doi.org/10.1155/2019/8385310

Research Article

Influence of Vibration Isolator Failure on Vehicle Operation Performance and Floating Slab Track Structure Vibration Reduction Effectiveness

Caiyou Zhao,[1,2] **Dongya Liu**,[1,2] **Xiaoming Zhang**,[1,2] **Qiang Yi**,[1,2] **Liuchong Wang**,[1,2] **and Ping Wang**[1,2]

[1]*Key Laboratory of High-speed Railway Engineering, Ministry of Education, Southwest Jiaotong University, Chengdu 610031, China*
[2]*School of Civil Engineering, Southwest Jiaotong University, Chengdu 610031, China*

Correspondence should be addressed to Liuchong Wang; wangliuchong@my.swjtu.edu.cn

Received 13 March 2019; Revised 30 April 2019; Accepted 27 May 2019; Published 20 June 2019

Academic Editor: Salvatore Russo

At present, steel-spring floating slabs have been widely used in urban rail transit to reduce the influence of ground vibration caused by vehicle operation on the surrounding environment. As a core part of vibration reduction for floating slab track, the steel-spring vibration isolator may fail in different forms during operation. In order to study the influence of vibration isolator failure on vehicle operation performance and floating slab track structure vibration reduction effectiveness, a rigid-flexible coupling dynamic model of vehicle-rail-floating slab track is established by multibody dynamics and finite element simulation, and the rationality of the model and its parameters is verified by comparing the theoretical calculation results with the measured data. Based on the model, the failure conditions of steel spring are simulated, considering the failure position and number of steel springs. The results show that the failures of steel-spring vibration isolators have a significant impact on operating safety and stability of vehicle, and the failure at end is more dangerous than that at midspan. In addition, it also changes the local restraint state of floating slab, resulting in the local vibration mode, which reduces the floating slab track structure vibration reduction effectiveness, mainly within 10 Hz. The different numbers of steel-spring failures will change the natural modal frequency of floating slab to varying degrees, which may cause the resonance of a certain frequency of the vehicle-track coupling system, leading to other track structure diseases.

1. Introduction

Urban rail transit has developed rapidly in recent years. However, in the meantime, ambient vibration and noise caused by subway operation also have a negative impact on residents' quality of work and life, normal use of vibration-sensitive equipment, and protection of ancient structures [1–3]. Therefore, vibration reduction is required in sensitive areas along subway lines. Vibration reduction measures can be divided into three types based on vibration source, propagation mode, and effectiveness: (i) active isolation of vibration source; (ii) termination of vibration propagation [4–9]; (iii) passive vibration isolation of vibrating object. First used for active vibration source isolation in Germany in 1965, floating slab tracks have good vibration reduction properties, and their use in controlling vibration from subways has since become more widespread [10, 11]. Among them, the steel-spring floating slab track has better vibration reduction effectiveness than other vibration reduction tracks, which can reach 25–40 dB [12, 13]. On the other hand, the design is mature, with advantages over other vibration reduction tracks such as lower operation, maintenance costs, and longer service life. Therefore, it is widely used in sensitive sections of urban rail transit.

The steel-spring floating slab track vibration isolation system consists mainly of the concrete bed slab, steel-spring vibration isolator, concrete floating slab, track structure, and shear hinge [14] (see Figure 1). Its basic principle for

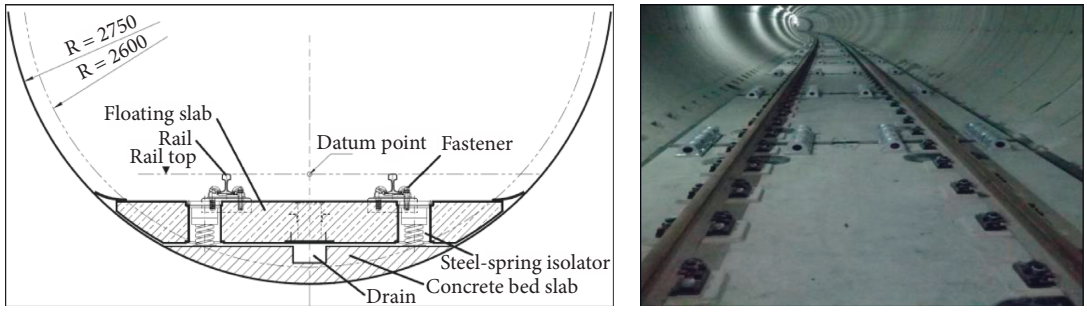

Figure 1: Structure of steel-spring floating slab track.

vibration reduction is to set a vibration isolator with a natural frequency far lower than the excitation frequency between the vibration source and foundation. The inertial force of the track slab mass offsets most of the dynamic load from the vehicle, and only the static load and a small amount of residual dynamic load are transferred to the vibration isolator and foundation after tuning, filtering, and energy absorption, thereby realizing vibration reduction [15]. It can be seen that the steel-spring vibration isolator is a discrete bearing structure for the floating slab track and a key part of vibration and noise reduction. It consists of inner and outer sleeves, a spiral steel spring, and viscous damping.

However, it has been found in the actual lines that steel-spring vibration isolator failures are subject to different conditions, as shown in Figure 2. Figure 2(a) shows some water seepage in the inspection tube, which is related to factors such as high rainfall or failure in the track drainage system. In this case, liquids can enter the inner sleeve and mix with the damping agent, causing loss of damping fluid in the sleeve, constant vibration isolator stiffness, and low damping. Figure 2(b) shows that suspended inner sleeve was caused by incorrect installation of the locking plate or by no or loosened locking bolt. Figure 2(c) shows that the steel-spring vibration isolator can break due to factors like fatigue or resonance, causing loss of damping fluid. The stiffness and damping of the steel-spring vibration isolator are both zero for the last two cases.

The steel-spring vibration isolator is a discrete supporting structure in the steel-spring floating slab track, and each steel-spring vibration isolator bears a considerable part of the load. Steel-spring vibration isolator failure, to a certain extent, destroys the uniformity and integrity of track structure and leads a sudden change of the railway tracks stiffness. Previous studies have shown that the abrupt stiffness change increases dynamic loads, asymmetric settlement, damage of track components, and maintenance costs. On the other hand, the sudden change of longitudinal support stiffness also causes easily low-frequency wheel-rail noise and induces low-frequency vibration of buildings or bridges near the lines [16, 17]. Therefore, it is necessary to study the influence of steel-spring failure on vehicle operation performance and floating slab track structure vibration reduction effectiveness for providing scientific and theoretical bases for daily maintenance and repair of track, focusing on the failure that the stiffness and damping completely lost.

The steel-spring vibration isolator failure is a kind of track bearing failure. At present, the studies on track bearing failure at home and abroad are mostly used to judge whether the failure occurs or the potential safety hazard, mainly including the failure of sleepers and fasteners. Esmaeili et al. established a numerical model for dynamic vehicle-rail interaction and analyzed the ground vibration caused by sleeper suspension of ballast track. The result showed that sleeper suspension of the ballast track could cause higher maximum ambient vibration velocity [2]. Lundqvist and Dahlberg analyzed the influence of sleeper suspension on wheel-rail interaction, showing that when a 1 mm suspension was caused between one sleeper and the ballast bed, the force acting between the adjacent sleeper and ballast bed increased by 70% [18]. Xiao et al. established a dissymmetric vehicle-track coupling dynamic model, and simulated fastener failure and studied its influence on dynamic train derailment assuming sudden change in the distribution of track stiffness in the longitudinal direction. The result showed that the dynamic train derailment index level increased continuously as the fastener condition ranged from almost loose to completely loose [19]. As a new vibration reduction measure, the steel-spring floating slab track has been widely used in recent years. Therefore, the studies on steel-spring vibration isolator failure are rare.

This paper establishes a rigid-flexible coupling dynamic model of vehicle-rail-floating slab track based on the numerical method and studies steel-spring failure according to the failure position and number of failed pairs, focusing on the influence of steel-spring vibration isolator failure on the operating performance of the vehicle and vibration reduction effectiveness of floating slab track. A section of a subway is studied to compare the theoretical calculation results with measured data under normal operation, verifying the rationality of the model and its parameters. At present, there are no detailed statistical summaries about the failure of steel-spring vibration isolator, so this paper carries out the idealized design of the failure condition of steel spring. The vehicle safety and stability evaluation indexes under the steel-spring failure design conditions are calculated based on the above model, and the influence of steel-spring vibration isolator failure

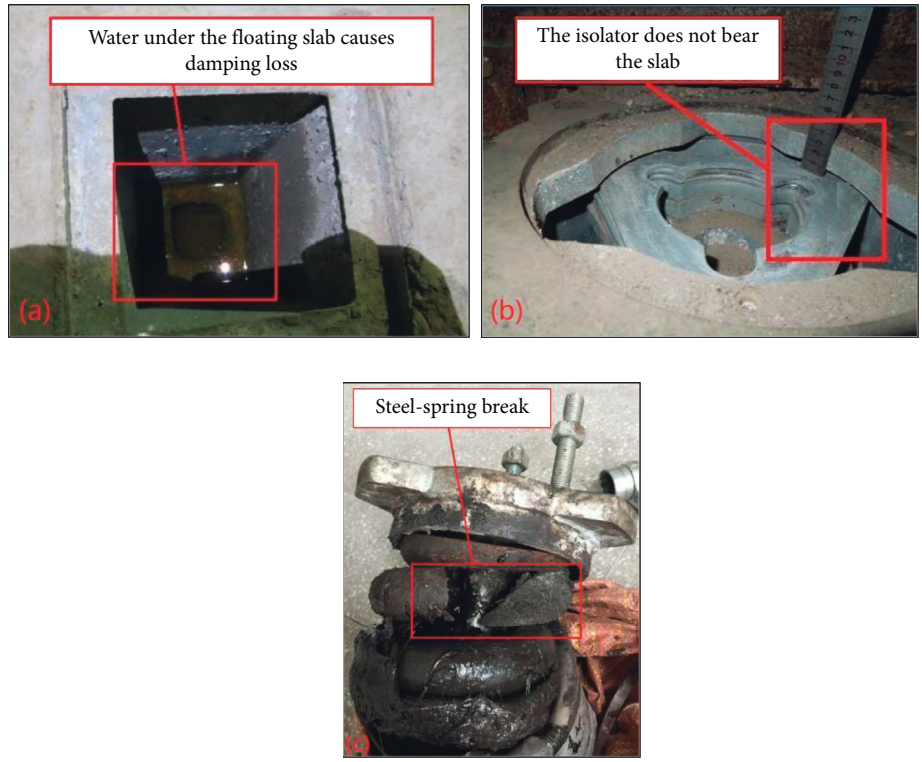

Figure 2: Vibration isolator failure. (a) Loss of damping fluid. (b) Inner sleeve suspension. (c) Broken steel spring.

on the operating performance of the vehicle is studied form the time- and frequency-domain perspectives. The Z vibration level of concrete bed slab under design condition is calculated in order to study the influence of steel-spring vibration isolator failure on the vibration reduction effectiveness of floating slab track, combined with modal analysis.

2. Rigid-Flexible Coupling Model

Dynamic rigid-flexible coupling model was generally made on the basis of joint finite element/dynamic software simulation. The coupling simulation model considered the vehicle as a multibody system, and the rail, floating slab and concrete bed slab were considered as flexible bodies, and the two were coupled by nonlinear wheel-rail contact.

2.1. Vehicle Model. A vehicle model was established according to the basic parameters of Type A subway vehicles. The single-car train model formed vibrations via 1 vehicle body, 2 bogies, and 4 wheel sets. The bogies were connected with the primary damping springs via the wheel sets, and the vehicle body and bogies were connected with the secondary dampers (see Figure 3). The single-car vehicle body had 5 independent degrees of freedom (DFs) at the central point: vertical and lateral displacement, rolling, pitch, and yaw, denoted as $\{V_c\} = \{Y_c, Z_c, \Phi_c, \beta_c, \Psi_c\}$, respectively. Each bogie had 5 independent DFs corresponding to the center of gravity, defined as $\{V_t\} = \{Y_t, Z_t, \Phi_t, \beta_t, \Psi_t\}$, just as with the vehicle body. The wheel set had 4 independent DFs and 2 dependent DFs, the former of which were longitudinal and lateral displacement, rolling, and yaw, denoted as $\{V_w\} = \{Y_w, Z_w, \Phi_w, \beta_w, \Psi_w\}$ (see Table 1 for the vehicle parameters).

2.2. Track Structure Model. The track system was simplified as a double-mass (floating slab and concrete bed slab) 3-layer (rail-floating slab-concrete bed slab-foundation) spring-damping vibrating structure, in which the rail, floating slab, and concrete bed slab were considered the flexible body. The rail was taken as Timoshenko beams on a discrete point-bearing foundation, involving vertical, lateral, and torsional vibration factors [20, 21]. The rail was connected to the floating slab via fasteners. Vertical equivalent stiffness and damping were denoted as K_z and C_z, respectively, and lateral equivalent stiffness and damping were denoted as K_s and C_s. The steel-spring vibration isolator was set between the floating slab and concrete basement, simulated as a linear spring. The vertical equivalent stiffness and damping were denoted as K_{fz} and C_{fz} and lateral equivalent stiffness and damping as K_{fy} and C_{fy}. The floating slabs were connected to each other via shear hinges. The concrete bed slab was connected to the foundation via bushing force elements. The vertical equivalent stiffness and damping were denoted as K_{bz} and C_{bz}, respectively, and lateral equivalent stiffness and damping as K_{by} and C_{by} (see Figure 4). The above structure's dynamic and geometric parameters are shown in Table 2. The grade six track irregularity PSD of the US Federal Railroad Administration (FRA) was adopted in this paper, considering track vertical irregularity and track lateral irregularity.

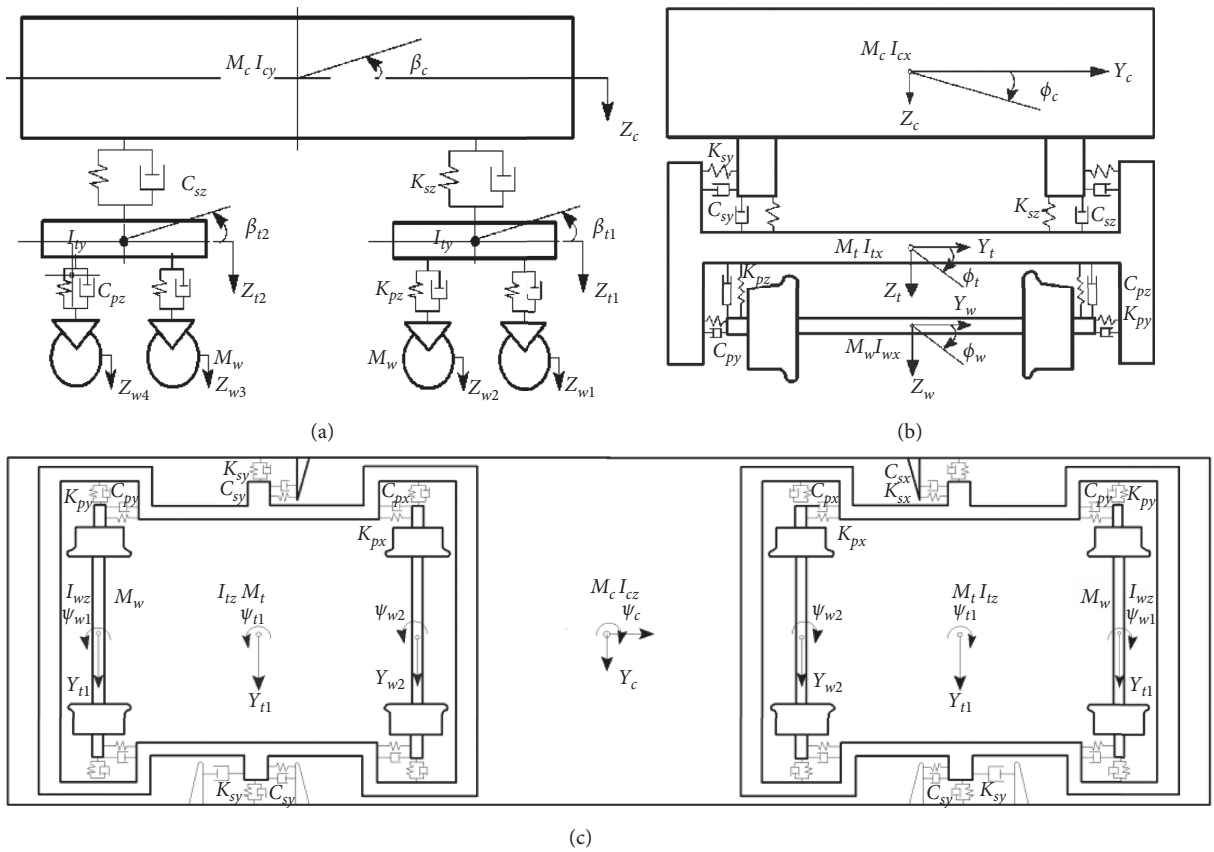

Figure 3: Dynamic vehicle model. (a) Side view. (b) Rear view. (c) Top view.

Table 1: Vehicle model parameters.

Item	Notation	Value	Unit
Mass of car body	M_c	34.69	t
Mass moment of inertia of car body around x-axis	I_{cx}	61	
Mass moment of inertia of car body around y-axis	I_{cy}	1835	t·m^2
Mass moment of inertia of car body around z-axis	I_{cz}	1816	
Mass of bogie	M_t	7.36	t
Mass moment of inertia of bogie around x-axis	I_{tx}	1.76	
Mass moment of inertia of bogie around y-axis	I_{ty}	2.18	t·m^2
Mass moment of inertia of bogie around z-axis	I_{tz}	4.00	
Mass of wheel set	M_w	1.90	t
Mass moment of inertia of wheel set around x-axis	I_{wx}	0.9	t·m^2
Mass moment of inertia of wheel set around z-axis	I_{wz}		
Stiffness of longitudinal secondary suspension system	K_{sx}	194	
Stiffness of lateral secondary suspension system	K_{sy}	194	kN/m
Stiffness of vertical secondary suspension system	K_{sz}	268	
Damping of vertical secondary suspension system	C_{sz}	80	kN·s/m
Stiffness of longitudinal primary suspension system	K_{px}	332	
Stiffness of lateral primary suspension system	K_{py}	332	kN/m
Stiffness of vertical primary suspension system	k_{pz}	550	
Damping of vertical primary suspension system	C_{pz}	6	kN·s/m

2.3. Validation of the Model with Experimental Data. A typical section of steel-spring floating slab track with better running condition was selected, and the design parameters of running vehicles and track were investigated, as shown in Tables 1 and 2. Based on the rigid-flexible coupling dynamic model of vehicle-rail-floating slab track established above, the floating slab vibration response of typical steel-spring floating slab track section at designed running speed was calculated. At the same time, the field experiment was conducted to measure the actual time-domain vibration response of floating slab under the same working condition. According to the position of the field measuring point, the

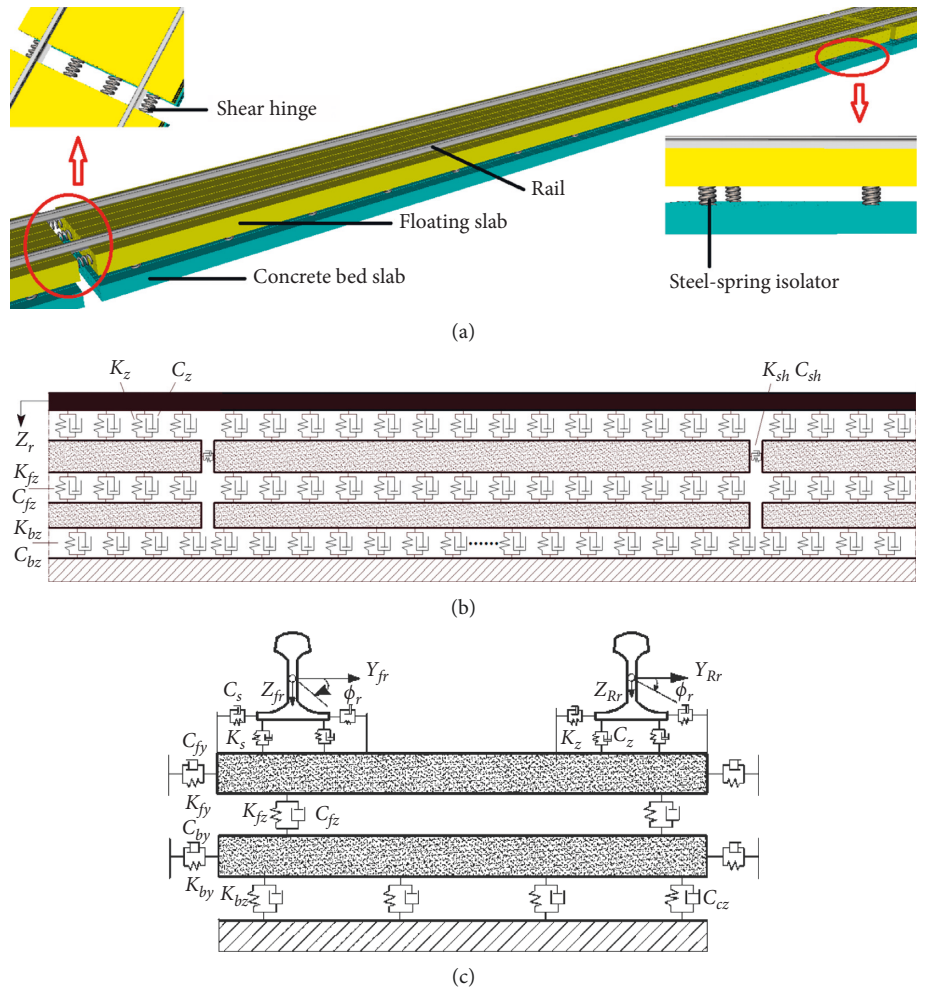

Figure 4: Simplified dynamic model of track structure. (a) Schematic diagram of track structure. (b) Side view. (c) Rear view.

Table 2: Track structure model parameters.

Structure	Item	Value	Unit
Rail	Elastic modulus	2.1×10^{11}	Pa
	Poisson's ratio	0.25	—
	Density	6064	kg/m^3
Fastener	Vertical stiffness	4×10^7	N/m
	Vertical damping	9.8×10^4	N·s/m
Floating slab	Length	25	m
	Width	2.4	m
	Height	0.4	m
	Elastic modulus	4.5×10^{11}	Pa
	Poisson's ratio	0.2	—
	Density	2500	kg/m^3
Shear hinge	Shear stiffness	5×10^9	N/m
Steel spring	Vertical stiffness	6.9×10^6	N/m
	Vertical damping	7.5×10^4	N·s/m
Concrete bed slab	Length	25	m
	Width	2.4	m
	Height	0.3	m
	Elastic modulus	4.5×10^{11}	Pa
	Poisson's ratio	0.2	—
	Density	2500	kg/m^3

vertical acceleration at the same position in the model was extracted. Comparing and analyzing the measured and theoretical values in time domains to verify the rationality of the rigid-flexible coupling dynamic model and its parameters, which could provide the reliable support for studying the influence of vibration isolator failure on vehicle operation performance and floating slab track structure vibration reduction effectiveness. Measuring point is arranged as shown in Figure 5.

Table 3 and Figure 6(a) compared the calculated results and measured results of floating slab vibration response in time domain. It could be seen that the two had fairly consistent time interval amplitude extremum, but their forms were slightly different because the measured results were affected by background vibration. The 1/3 octave vertical frequency-weighted vibration accleration Z vibration level (VL_z) obtained by processing the time-domain data in Figure 6(a) shall be analyzed comparatively, as shown in Figure 6(b). From the measured results, it could be seen that the main frequency of vertical vibration of steel-spring floating slab at the field measuring point was 6.3–100 Hz, and the advanced peaks are at the same central frequencies

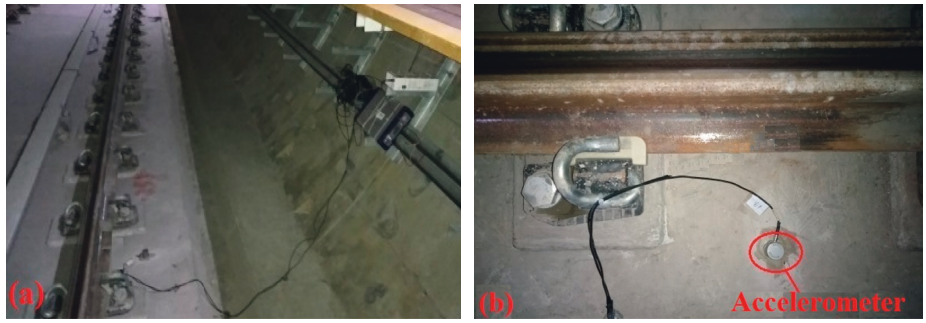

Figure 5: Position of measuring point at floating slab.

Table 3: Comparisons between the maximum and minimum of calculated and measured results.

Conditions results	Maximum (m/s^2)	Minimum (m/s^2)
Calculated result	5.45	−4.95
Measured result	4.80	−4.70

which are 12.5 Hz and 63 Hz, respectively. The larger one was located at 63 Hz of the central frequency, which was caused by inducing wheel-rail resonance. The calculated results are smaller above 125 Hz probably because the length of the minimum wavelength of track irregularity is not short enough. However, it does not affect the later analysis results. Similarly, the calculated results showed that the vertical vibration acceleration level of the steel-spring floating slab had a good coincidence, and the dynamic rigid-flexible coupling model had good calculation accuracy.

3. Calculation Conditions

This paper simulates the operating conditions of a rail train running on a floating slab track at 80 km/h and studies the failure position and number. However, there are no detailed statistic induction about the failure conditions of steel spring on actual operation line presently so that this paper makes an idealized design of steel-spring failure conditions and considers the most dangerous conditions, which are the inner sleeve suspension and direct steel-spring breakage (see Figures 2(b) and 2(c)). Moreover, the failure on one side of the rail was calculated, which had no obvious influence on vehicle operation performance and floating slab track structure vibration reduction effectiveness. Therefore, this paper only considered paired failure of steel spring in the design of working conditions. As for the longitudinal periodic distribution characteristics of the steel-spring floating slab, two points were considered with regard to steel-spring failure: the failure position and number of failed steel springs. The failure position was set at the end and middle portions of the floating slab, while 2, 4, and 6 pairs of steel-spring failures in the track direction from the failure position were considered for the steel-spring failure number (see Figure 7). All steel springs with the same number were considered to fail at the same time. Table 4 shows the numbers of steel-spring failure calculation conditions.

4. Calculated Results and Analysis

4.1. Impact of Steel-Spring Failure on Operating Safety. Safety indices such as the vehicle derailment coefficient Q/P, normal wheel-rail force P, and wheel unloading rate $\Delta P/P$ under different steel-spring failure positions and numbers of pairs were calculated using the dynamic vehicle-rail-floating slab track model established above. Steel-spring failure only has significant influence on the failed sections, with little influence on distant parts; therefore, only data from within 1.5 s–4.5 s of passage through the failed sections were analyzed.

4.1.1. Steel-Spring Failure Position. Figure 8 shows the vehicle operation safety parameters of the 6 steel-spring pairs in the case of breakage at the slab end and midspan.

As shown in Figure 8, steel-spring failure increased the vehicle operation safety parameters in different degrees. When the steel spring failed at the slab end, the maximum derailment coefficient was slightly larger than that failed at the midspan, increased by 1.2 times, but both were within the safe range of it. Under normal conditions, the maximum wheel unloading rate was 0.152 and the maximum normal wheel-rail force was 84.11 kN. When the steel spring failed at the slab end, the maximum wheel unloading rate was 0.243 and the maximum normal wheel-rail force was 90.76 kN. When the steel spring failed at the midspan, the maximum wheel unloading rate was 0.180 and the maximum normal wheel-rail force was 86.15 kN. When the steel spring failed at the slab end and midspan, respectively, compared to normal conditions, the wheel unloading rate increased by 59.9% and 18.4%, respectively, and the normal wheel-rail force increased by 7.9% and 2.4%, respectively. Heavy positive wheel-rail pressure could cause damage such as flat spots, fractured rail head, bolt hole cracks, and broken fishplates, indirectly influencing operational safety [19].

4.1.2. Number of Steel-Spring Failures. Figure 9 shows the vehicle operation safety parameters in the time domain when the slab end was subject to 2, 4, and 6 pairs of steel-spring break failures.

As shown in Figure 9, the derailment coefficient, wheel unloading rate, and normal wheel-rail force increased

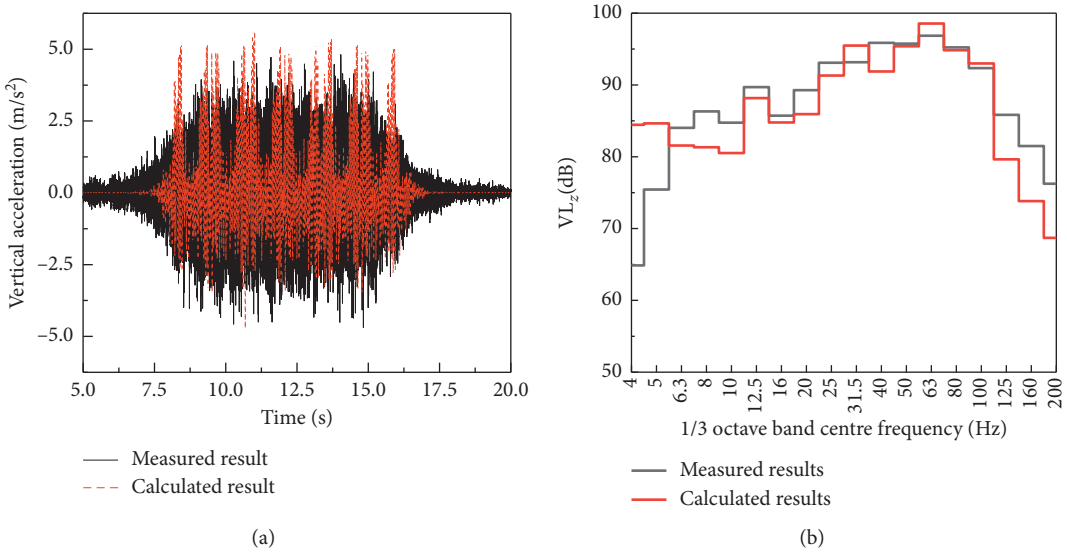

Figure 6: Comparison of calculated and measured results of floating slab. (a) Time domain. (b) Frequency domain.

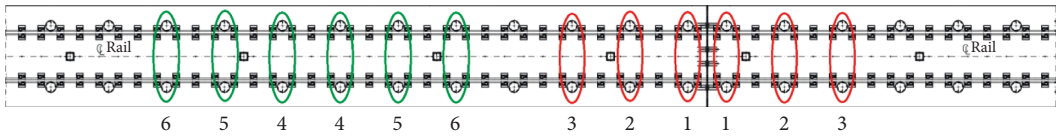

Figure 7: Steel-spring failure conditions.

Table 4: Calculation conditions of steel-spring failure.

Failure position	Number of failures	Failure degree	
		No failure	Breakage
End of floating slab	2 pairs	S	S_{11}
	4 pairs		S_{12}
	6 pairs		S_{13}
Midsection of floating slab	2 pairs		S_{21}
	4 pairs		S_{22}
	6 pairs		S_{23}

continuously as the vehicle passed the failure positions with the increasing number of failures. Under normal conditions, the maximum values of derailment coefficient, wheel unloading rate, and normal wheel-rail force were 0.059, 0.152, and 84.11 kN, respectively. Going from 0 to 2, 4, and 6 pairs of failures, the maximum derailment coefficients were 0.060, 0.061, and 0.065, respectively, increased by 1.7%, 3.4%, and 10.2%. The maximum wheel unloading rates were 0.150, 0.185, and 0.243, respectively, decreased by 1.3% and then increased by 21.7% and 60.0%. The maximum normal wheel-rail forces were 83.92 kN, 86.51 kN, and 90.76 kN, respectively, decreased by 0.23% and then increased by 2.9% and 7.9%. It could be seen that there was a nonlinear relationship between the vehicle operation safety indices and the number of steel-spring failures. A few steel-spring failures had less impact, and with the increase of failure numbers, the operation safety indices could increase sharply, threatening the safety of the train.

4.2. Influence of Steel-Spring Failure on Vehicle Stability. Stability parameters such as vertical vehicle body acceleration and the lateral and vertical Sperling stability indices under different steel-spring failure positions and numbers of pairs were calculated using the dynamic vehicle-rail-floating slab track model established above. Time- and frequency-domain analyses were made on the calculated results in order to analyze the influence of steel-spring failure on vehicle stability.

4.2.1. Steel-Spring Failure Position. Figure 10 shows vertical vehicle body acceleration in the time domain, the extracted vertical vehicle body acceleration in the frequency domain below 20 Hz, and the lateral and vertical Sperling stability indices, when 6 pairs of steel spring were subject to slab end and midspan breakage.

As shown in Figure 10, the point of steel-spring failure significantly influenced the vertical acceleration. The vertical acceleration sharply increased when vehicle passed through the failure section and changed more sharply when failure occurred at the slab end. Portions distant from the failure section were almost not affected. The PSD of the vertical vehicle body acceleration below 10 Hz was obviously larger than that beyond 10 Hz, significantly increased due to the steel-spring failure. It could be seen that the floating slab track had low vibration reduction effectiveness for the vibration below 10 Hz which was sensitive for precision instruments, buildings, and human bodies, and steel-spring failure would aggravate the vibration below 10 Hz, especially failed at the slab end.

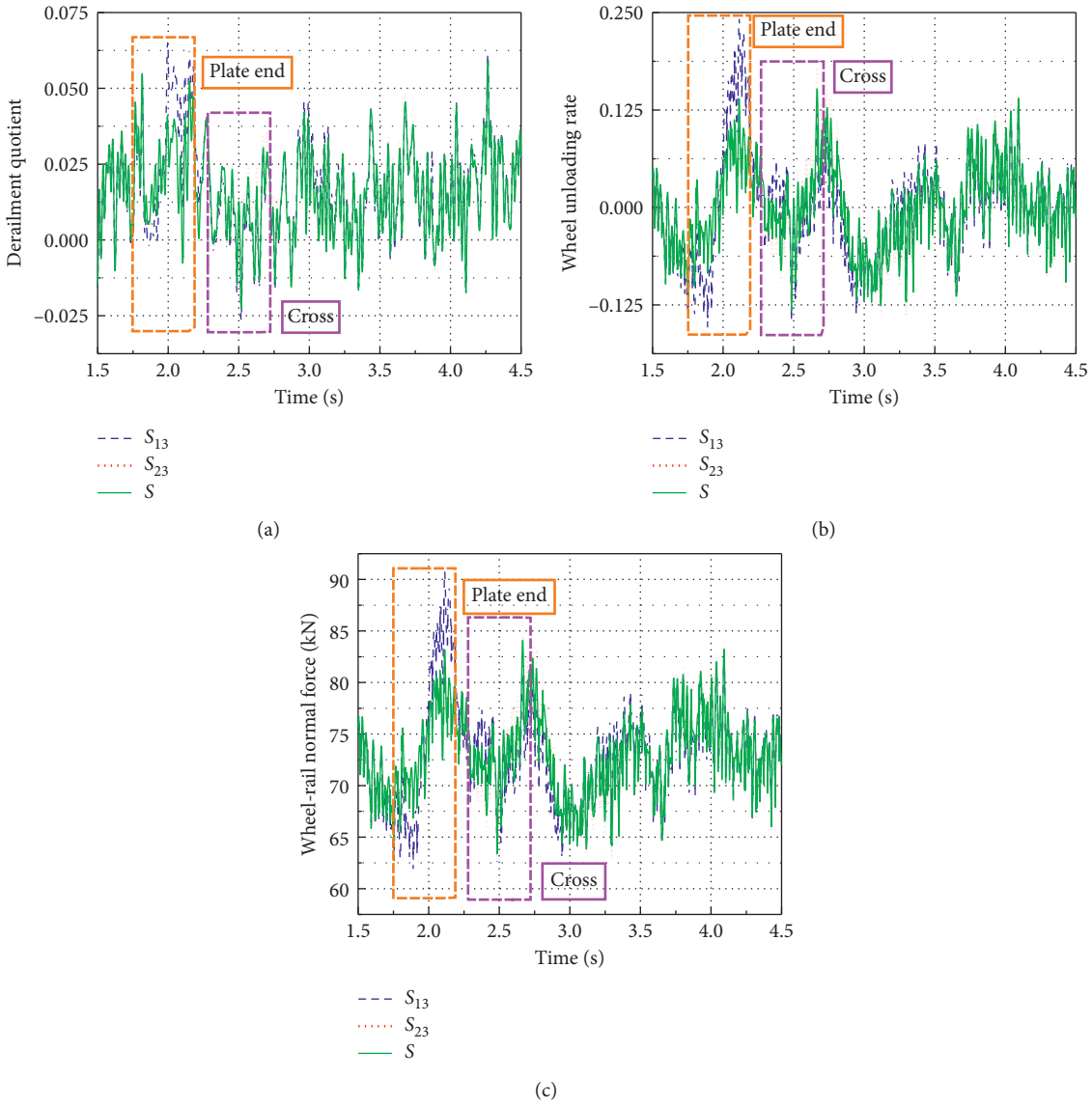

Figure 8: Influence of steel-spring failure position on vehicle operation safety.

Under normal conditions, the maximum vertical vehicle body acceleration was 0.245 m/s^2 and the lateral and vertical Sperling stability indexes were 2.284 and 1.271, respectively. When the steel spring, respectively, failed at the slab end and midspan, the maximum vertical vehicle body accelerations were 0.808 m/s^2 and 0.310 m/s^2, which were 3.30 and 1.27 times of normal conditions, respectively. The lateral Sperling stability indexes were 2.296 and 2.230, respectively, and compared to normal conditions, the former increased by 0.5% and the latter decreased by 2.4%. The vertical Sperling stability indexes were 1.916 and 1.552, which increased by 50.7% and 22.1% compared with normal conditions, respectively. It could be seen that when steel-spring failure occurred at the slab end, the vertical vehicle body acceleration, PSD of the vertical vehicle body acceleration, and vertical Sperling stability index were larger than that failed in the midspan. In addition, the lateral Sperling stability index was almost unaffected because the lateral restraint of steel spring was far less than the vertical restraint and the reduction of lateral restraint caused by the steel-spring failure was almost negligible compared with the overall lateral restraint of structure. The maximum Sperling stability index was 2.296, which would not affect the vehicle stability, without considering other track disturbances. Previous studies had shown that when track was influenced by other disturbances, the transient response of vehicle/track system in the failure section would become larger [18, 22].

4.2.2. Number of Steel-Spring Failures. Figure 11 shows vertical vehicle body acceleration in the time domain, the extracted vertical vehicle body acceleration in the frequency domain below 20 Hz, and the lateral and vertical Sperling stability indices, when 2, 4, and 6 pairs of steel springs were subject to slab end failures.

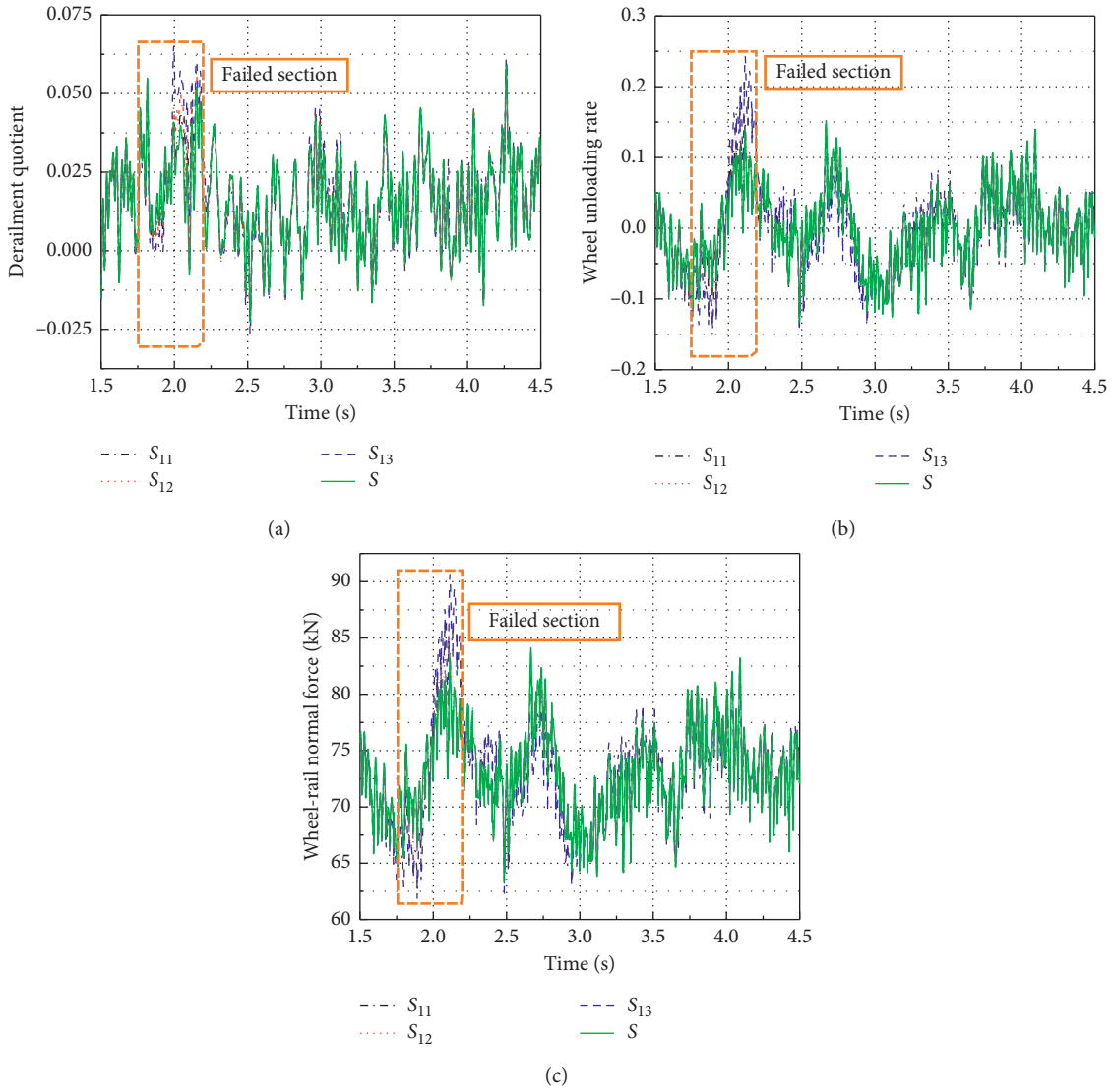

Figure 9: Influence of number of steel-spring failures on vehicle operation safety.

As shown in Figure 11, the numbers of steel-spring failures had little influence on the shape of vertical acceleration but had a significant influence on the amplitude. Under normal condition, the maximum vertical vehicle body acceleration was 0.204 m/s^2 and the vertical Sperling stability index was 1.271. Going from 0 to 2, 4, and 6 pairs of failures, the maximum vertical vehicle body acceleration was 0.208 m/s^2, 0.466 m/s^2, and 0.808 m/s^2, respectively, which increased by 1.02, 2.28, and 3.96 times, and the vertical Sperling stability index was 1.312, 1.548, and 1.916, which increased by 3.2%, 21.8%, and 50.7%, respectively. The maximum vertical vehicle body acceleration and vertical Sperling stability index increased nonlinearly with the increase of the numbers of steel-spring failures, while the lateral Sperling stability index did not change significantly.

4.3. Influence of Steel-Spring Failure on Vibration Reduction Effectiveness of Floating Slab Track. In this paper, the vertical acceleration Z vibration level of concrete bed slab was used as the evaluation index for vibration reduction effectiveness and the frequency weighting grid recommended by the IS02631 standard was adopted [23]. The frequency range was considered to be 4 to 200 Hz.

Vertical acceleration Z vibration level was expressed as

$$\mathrm{VL}_Z = 20\lg\frac{a_{ez}}{a_0}, \tag{1}$$

where a_{ez} referred to the Z-weighted acceleration effective value of whole body vibration in m/s^2 and a_0 referred to the reference acceleration, which is usually 10^{-6} m/s^2.

4.3.1. Steel-Spring Failure Position. The vertical acceleration Z vibration level at midspan and end of concrete bed slab under different steel-spring failure positions was calculated using the dynamic vehicle-rail-floating slab track model established above. The results are shown in Figure 12. Meanwhile, the vibration mode of single-span floating slab track structure was analyzed, considering the longitudinal

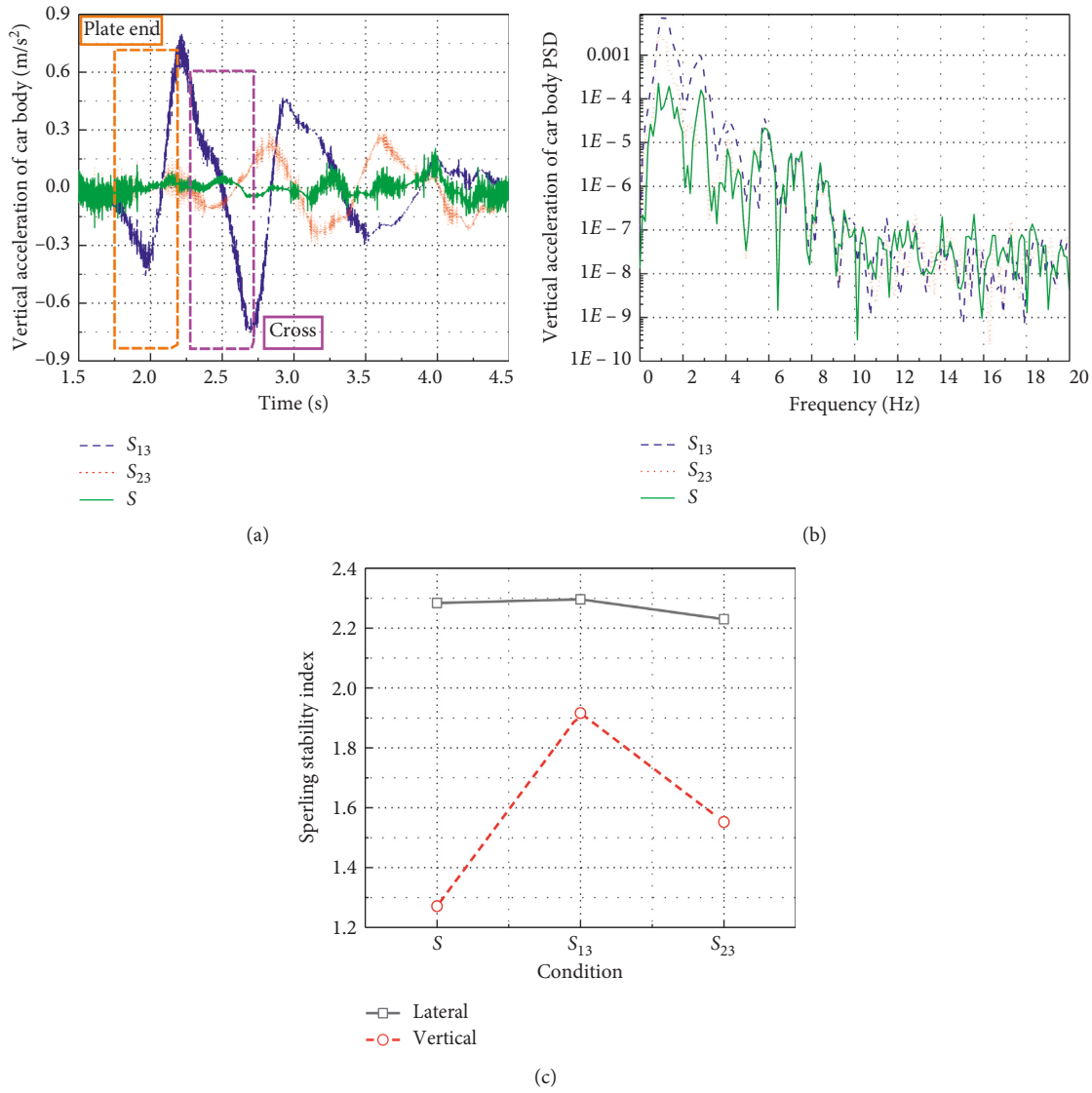

Figure 10: Influence of steel-spring failure position on vehicle operation stability.

periodic variation. The boundary conditions were set to simulate multiple spans.

It was generally believed that steel-spring failure leaded to the decrease of overall stiffness so that the vibration reduction effectiveness of floating slab track should be enhanced. However, as shown in Figure 12, when failure occurred at the slab end, the vertical acceleration Z vibration level at midspan and end of concrete bed slab increased significantly in the range of 4–6.3 Hz and 4–12.5 Hz, respectively, and the maximum Z vibration level of 115.14 dB existed in the end of the concrete bed slab at 4 Hz. When failure occurred at the middle, the vertical acceleration Z vibration level at midspan generally increased, especially in the frequency range of 4–10 Hz, while the vertical acceleration Z vibration level at end did not change much. The maximum Z vibration level of 98.56 dB existed in the midspan of the concrete bed slab at 10 Hz. The maximum Z vibration level was related to the local vibration mode of floating slab track, caused by the decrease of local restraint ability of floating slab track, and decreased the vibration reduction effectiveness of floating slab track, as shown in Figure 13. It could be seen that the steel-spring failure mainly affected the vibration reduction effectiveness of low-frequency vibration of about 10 Hz, which was very sensitive to precision instruments, buildings, and human bodies. On the other hand, the steel-spring failure at end would reduce the vibration reduction effectiveness of the end and midspan of floating slab track, while the steel-spring failure at midspan would only have a negative impact on the vibration reduction effect of midspan.

4.3.2. Number of Steel-Spring Failures. Figure 14 shows the vertical acceleration Z vibration level at midspan and end of concrete bed slab when 2, 4, and 6 pairs of steel-springs were subject to slab end failures. Figure 15 shows the local vibration mode under different failure conditions.

As shown in Figure 14, the 2 pairs of failures had little effect on vertical acceleration Z vibration level at midspan of

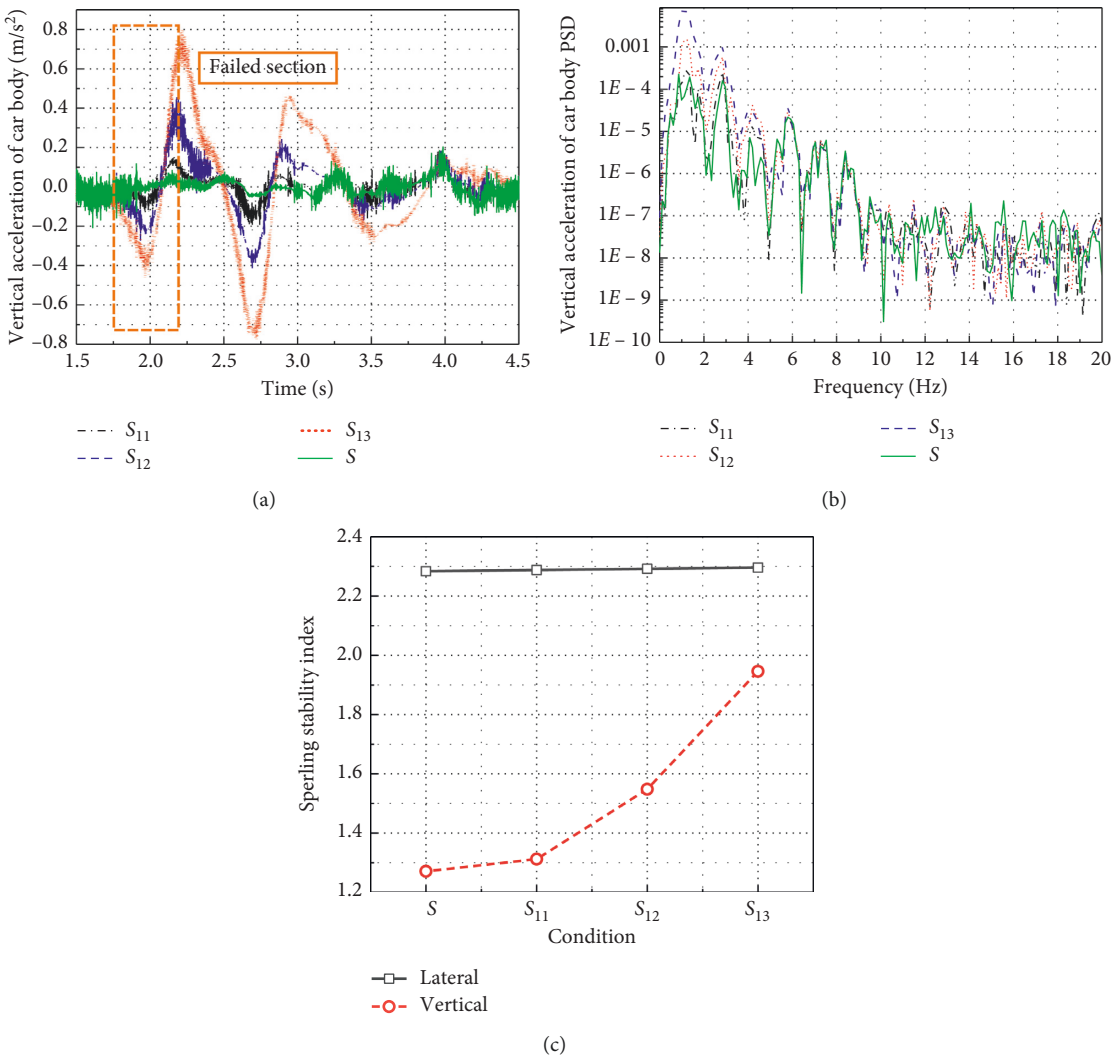

Figure 11: Influence of number of steel-spring failures on vehicle operation stability.

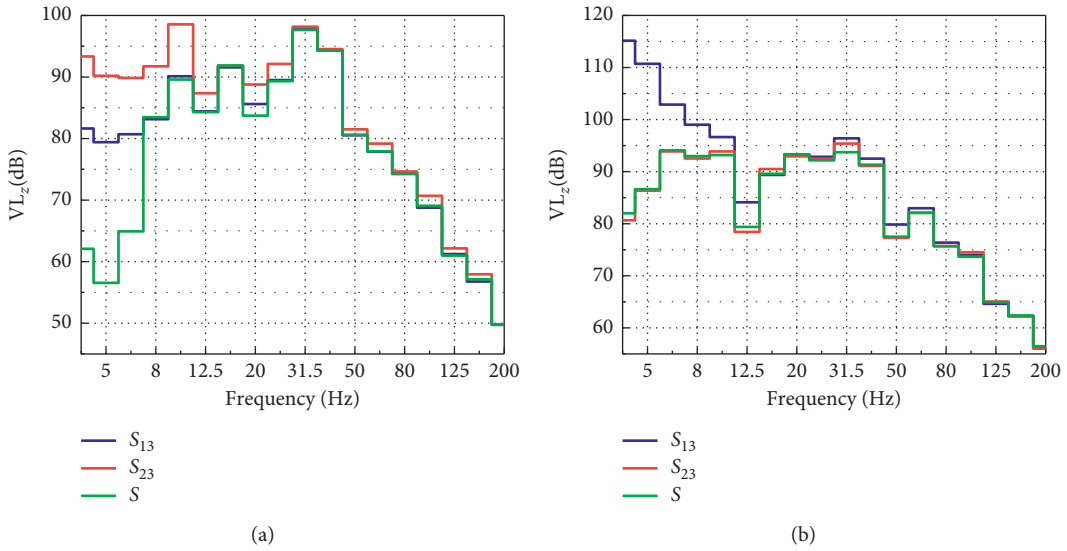

Figure 12: Influence of steel-spring failure position on vibration reduction effectiveness. (a) VL_z at midspan. (b) VL_z at end of concrete bed slab.

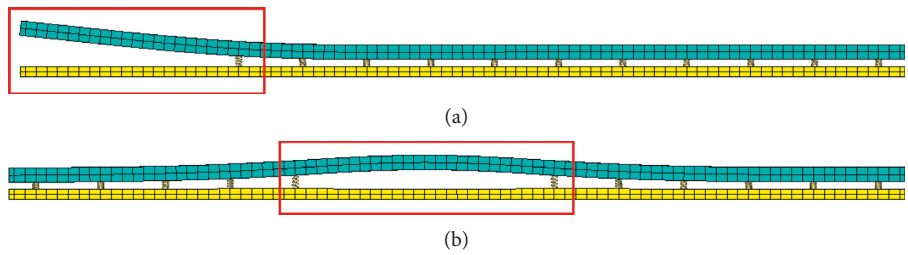

Figure 13: Influence of steel-spring failure position on local vibration mode. (a) $S_{13}=$, $f=3.4$ Hz. (b) $S_{23}=$, $f=9.5$ Hz.

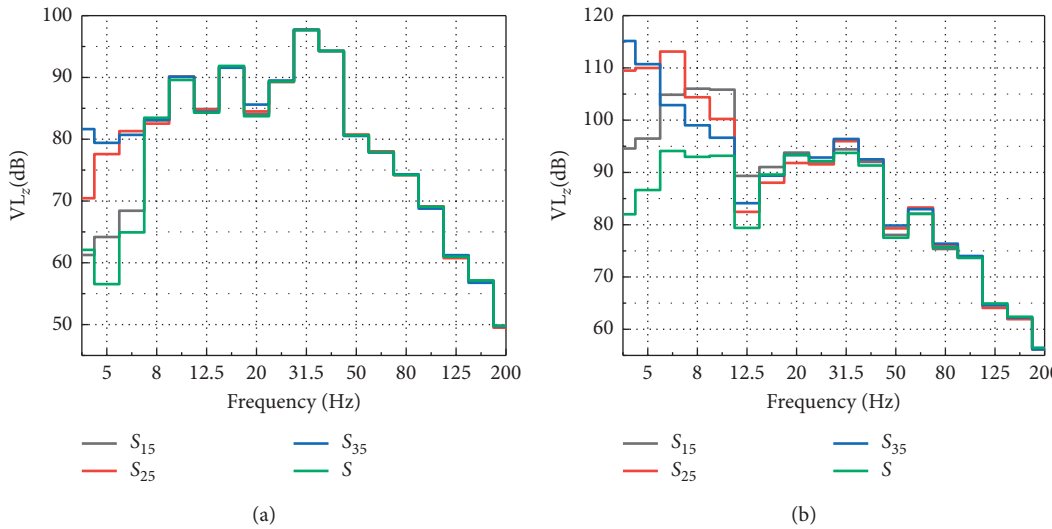

Figure 14: Influence of number of steel-spring failures on vibration reduction effectiveness. (a) VL_z at midspan. (b) VL_z at end of concrete bed slab.

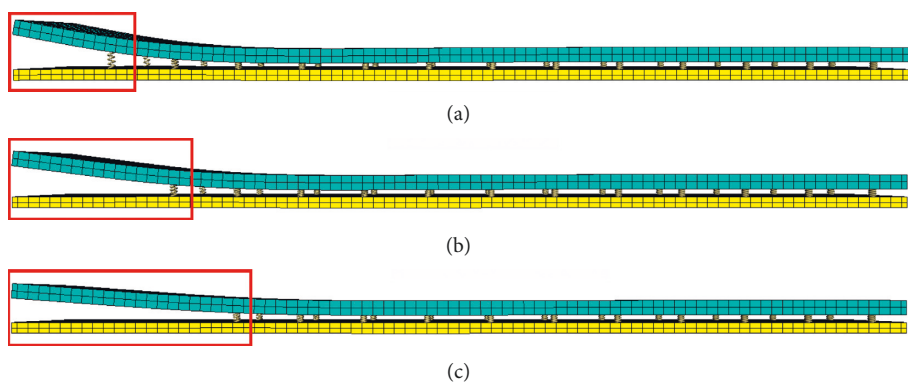

Figure 15: Influence of number of steel-spring failures on local vibration mode. (a) S_{15}, $f=9.6$ Hz. (b) S_{25}, $f=5.4$ Hz. (c) S_{35}, $f=3.4$ Hz.

concrete bed slab, but vertical acceleration Z vibration level at end was larger than other failure conditions in the frequency range of 8–12.5 Hz, which was due to the existence of local vibration mode in the end of the slab at 9.6 Hz (see Figure 15(a)). When the steel spring failed 4 pairs, the vertical acceleration Z vibration level at midspan of concrete bed slab was almost equal to that which failed 6 pairs. In addition, the vertical acceleration Z vibration level at end was larger than that under other working conditions because of the local vibration mode of 5.4 Hz (see Figure 15(b)). When the steel-spring failed 6 pairs, the vertical acceleration Z vibration level at midspan and end of concrete bed slab was the largest in all working conditions at about 4 Hz and 5 Hz, respectively, caused by the local vibration mode at 3.4 Hz, as shown in Figure 15(c). It could be seen that there is no linear relationship between the vibration reduction effectiveness of floating slab track structure and the number of steel-spring failure. In a certain frequency range, a few

steel-spring failures might be more disadvantageous because of the local vibration mode, which varied with the number of failures.

5. Conclusions

In order to study the influence of steel-spring failure on vehicle operation safety/stability and vibration reduction effectiveness of floating slab track, a dynamic vehicle-rail-floating slab track coupling model was established based on rigid-flexible coupling theory. The steel-spring failure was simulated by assuming that the stiffness and damping of vibration isolators become zero suddenly in the longitudinal distribution direction. Considering the failure position and number of steel-spring failures, the following conclusions are drawn:

(1) By comparing the numerical simulation results with the field measured data, it was found that the vibration response of floating slab was consistent with time domain, which verifies the rationality of the vehicle-rail-floating slab track coupling dynamic model and its parameters.

(2) The steel-spring failure increased the vehicle operation indices of safety and stability in varying degrees and mainly occurred when vehicle passed through the failure section, decreasing the vehicle operation performance. In addition, it also resulted in the local vibration mode of floating slab, reducing the vibration reduction effectiveness of floating slab track within 10 Hz.

(3) When steel-spring failure occurred at the slab end and midspan, compared to normal conditions, the maximum wheel unloading rate increased by 59.9% and 18.4%, respectively. The maximum normal wheel-rail force increased by 7.9% and 2.4%, respectively. The maximum vertical vehicle body acceleration increased by 3.30 and 1.27 times, and the vertical Sperling stability index increased by 50.7% and 22.1%, respectively. It showed that when steel-spring failure occurred at the slab end, the vehicle operation safety and stability indices were larger than that failed in the midspan.

(4) When steel-spring failure occurred at the slab end, the vertical acceleration Z vibration level at midspan and end of concrete bed slab increased significantly in the range of 4–6.3 Hz and 4–12.5 Hz, respectively, and the maximum Z vibration level of 115.14 dB existed in the end of concrete bed slab at 4 Hz. When failure occurred at the middle, the vertical acceleration Z vibration level at midspan generally increased, especially in the frequency range of 4–10 Hz, while the vertical acceleration Z vibration level at end did not change much. The maximum Z vibration level of 98.56 dB existed in the midspan of the concrete bed slab at 10 Hz. Therefore, the railway engineering department should pay attention to the steel-spring failure in routine maintenance, especially the failure at the floating slab end.

(5) Going from 0 to 2, 4, and 6 pairs of steel-spring failures at the slab end, compared to normal conditions, the maximum derailment coefficient increased by 1.7%, 3.4%, and 10.2%, respectively. The maximum wheel unloading rate decreased by 1.3% and then increased by 21.7% and 60.0%. The maximum normal wheel-rail force decreased by 0.23% and then increased by 2.9% and 7.9%. The maximum vertical vehicle body acceleration increased by 1.02, 2.28, and 3.96 times, and the vertical Sperling stability index increased by 3.2%, 21.8%, and 50.7%, respectively. It could be seen that with the increase of the number of steel-spring failures, the vehicle operation safety and stability indices increased nonlinearly, which had a negative impact on the vehicle operation performance.

(6) Going from 2 to 4 and 6 pairs of steel-spring failures at the slab end, the natural frequencies of local vibration modes were 9.6 Hz, 5.4 Hz, and 3.4 Hz, respectively, which would reduce the vibration reduction effectiveness of floating slab track around its natural frequency. Therefore, the adverse effects of steel-spring failures could not be evaluated simply by the number of steel-spring failures. In routine maintenance, no matter the number of steel-spring failures, the relevant departments should pay attention to it.

Data Availability

The data used to support the findings of this study are available from the corresponding author upon request.

Conflicts of Interest

The authors declare that they have no conflicts of interest.

Acknowledgments

Thanks are due to the National Key Research and Development Program of China (2016YFE0205200) and the National Natural Science Foundation of China (NNSFC) (51425804) for the research grant awarded to Caiyou Zhao and the Doctoral Innovation Fund Program of Southwest Jiaotong University and the Research Fund for Key Research and Development Projects in Sichuan Province (2017GZ0373).

References

[1] L. Schillemans, "Impact of sound and vibration of the North-South high-speed railway connection through the city of Antwerp Belgium," *Journal of Sound and Vibration*, vol. 267, no. 3, pp. 637–649, 2003.

[2] M. Esmaeili, S.-A. Mosayebi, and J.-A. Zakeri, "Ground-borne vibrations caused by unsupported railway sleepers in ballasted tracks," *Procedia Engineering*, vol. 199, pp. 2645–2650, 2017.

[3] K. Alten, H. Friedl, and R. Flesch, "Calculating ground-borne noise from ground-borne vibra-tion–a Comparison of

different approaches," in *Proceedings of the ISMA*, Leuven, Belgium, September 2010.

[4] P. Zoccali, G. Cantisani, and G. Loprencipe, "Ground-vibrations induced by trains: filled trenches mitigation capacity and length influence," *Construction and Building Materials*, vol. 74, no. 74, pp. 1–8, 2015.

[5] M. Adam and O. Von Estorff, "Reduction of train-induced building vibrations by using open and filled trenches," *Computers & Structures*, vol. 83, no. 1, pp. 11–24, 2005.

[6] A. Dijckmans, A. Ekblad, A. Smekal, G. Degrande, and G. Lombaert, "Efficacy of a sheet pile wall as a wave barrier for railway induced ground vibration," *Soil Dynamics and Earthquake Engineering*, vol. 84, pp. 55–69, 2016.

[7] P. Persson, K. Persson, and G. Sandberg, "Numerical study of reduction in ground vibrations by using barriers," *Engineering Structures*, vol. 115, pp. 18–27, 2016.

[8] G. Gao, N. Li, and X. Gu, "Field experiment and numerical study on active vibration isolation by horizontal blocks in layered ground under vertical loading," *Soil Dynamics and Earthquake Engineering*, vol. 69, pp. 251–261, 2015.

[9] A. Dijckmans, P. Coulier, J. Jiang et al., "Mitigation of railway induced ground vibration by heavy masses next to the track," *Soil Dynamics and Earthquake Engineering*, vol. 75, pp. 158–170, 2015.

[10] J. T. Nelson, "Recent developments in ground-borne noise and vibration control," *Journal of Sound and Vibration*, vol. 193, no. 1, pp. 367–376, 1996.

[11] P. Grootenhuis, "Floating track slab isolation for railways," *Journal of Sound and Vibration*, vol. 51, no. 3, 1977.

[12] J. Wang and T. Wu, "On vibration isolation performance of floating slab track," *Journal-Shanghai Jiaotong University-Chinese Edition*, vol. 41, no. 6, p. 1021, 2007.

[13] C. Kuo, C. Huang, and Y. Chen, "Vibration characteristics of floating slab track," *Journal of Sound and Vibration*, vol. 317, no. 3–5, pp. 1017–1034, 2008.

[14] A. R. Crockett and J. R. Pyke, "Viaduct design for minimization of direct and structure-radiated train noise," *Journal of Sound and Vibration*, vol. 231, no. 3, pp. 883–897, 2000.

[15] G. P. Wilson, H. J. Saurenman, and J. T. Nelson, "Control of ground-borne noise and vibration," *Journal of Sound and Vibration*, vol. 87, no. 2, pp. 339–350, 1983.

[16] X. B. Xiao, X. S. Jin, and Z. F. Wen, "Effect of track support failure on dynamic response of tangent track," *Chinese Journal of Theoretical and Applied Mechanics*, vol. 40, no. 1, pp. 67–78, 2008, in Chinese.

[17] B. Y. An, D. L Ma, P. Wang et al., "Assessing the fast non-Hertzian methods based on the simulation of wheel–rail rolling contact and wear distribution," *Proceedings of the Institution of Mechanical Engineers, Part F: Journal of Rail and Rapid Transit*, article 732799344, 2019.

[18] A. Lundqvist and T. Dahlberg, "Load impact on railway track due to unsupported sleepers," *Proceedings of the Institution of Mechanical Engineers, Part F: Journal of Rail and Rapid Transit*, vol. 219, no. 2, pp. 67–77, 2005.

[19] X. B. Xiao, X. S. Jin, and Z. F. Wen, "Influence of rail fastener failure on vehicle dynamic derailment," *Journal of Traffic and Transportation Engineering*, vol. 1, p. 1, 2006.

[20] X. Sheng, M. Li, C. Jones, and D. J. Thompson, "Using the fourier-series approach to study interactions between moving wheels and a periodically supported rail," *Journal of Sound and Vibration*, vol. 303, no. 3–5, pp. 873–894, 2007.

[21] S. Zhang, X. Xiao, Z. Wen, and X. Jin, "Effect of unsupported sleepers on wheel/rail normal load," *Soil Dynamics and Earthquake Engineering*, vol. 28, no. 8, pp. 662–673, 2008.

[22] S. L. Grassie and S. J. Cox, "The dynamic response of railway track with unsupported sleepers," *Proceedings of the Institution of Mechanical Engineers, Part D: Transport Engineering*, vol. 199, no. 24, pp. 123–136, 1985.

[23] C. Lalanne, *Mechanical Vibration and Shock*, John Wiley & Sons, Hoboken, NJ, USA, 1986.